Modelling the Characteristic Residues of Chlorophyll f Synthase (ChlF) from Halomicronema Hongdechloris to Determine Its Reaction Mechanism

Min Chen * , Artur Sawicki , Fanyue Wang

Posted Date: 30 August 2023

doi: 10.20944/preprints202308.2051.v1

Keywords: Photosystem II; chlorophyll; free radical; cyanobacteria; oxygen evolution centre; chlorophyll f biosynthesis

Article

Modelling the Characteristic Residues of Chlorophyll *f* Synthase (ChlF) from *Halomicronema Hongdechloris* to Determine Its Reaction Mechanism

Min Chen [1,*], Artur Sawicki [1,2] and Fanyue Wang [1]

[1] School of Life and Environmental Sciences, University of Sydney, Sydney, NSW 2006, Australia
[2] School of Biotechnology and Biomolecular Sciences, University of New South Wales, NSW 2052, Australia (current working address)
* Correspondence: min.chen@sydney.edu.au; Tel.: (+61 2 9036 5006)

Abstract: Photosystem II (PSII) is a quinone-utilizing photosynthetic system that converts light energy into chemical energy and catalyzes water splitting. PsbA (D1) and PsbD (D2) are the core subunits of the reaction center that provide most of the ligands to redox active cofactors and exhibit photooxidoreductase activities that convert quinone and water into quinol and dioxygen. The performed analysis explored the putative uncoupled electron transfer pathways surrounding P_{680}^{+} induced by far-red light (FRL) based on photosystem II (PSII) complexes containing substituted D1 subunits in *Halomicronema hongdechloris*. Chlorophyll *f*-synthase (ChlF) is a D1 protein paralog. Modelling PSII-ChlF complexes determined several key protein motifs of ChlF. The PSII complexes included a dysfunctional Mn_4CaO_5 cluster where ChlF replaced the D1 protein. We propose the mechanism of chlorophyll *f* synthesis from chlorophyll *a* via free radical chemistry in an oxygenated environment created by over-excited pheophytin *a* and an inactive water splitting reaction due to an uncoupled Mn_4CaO_5 cluster in PSII-ChlF complexes. The role of ChlF in the formation of an inactive PSII reaction center is under debate and putative mechanisms of chlorophyll *f* biosynthesis are discussed.

Keywords: Photosystem II; chlorophyll; free radical; cyanobacteria; oxygen evolution centre; chlorophyll *f* biosynthesis

1. Introduction

Photosynthesis is a fundamental process that converts light energy into chemical energy. Oxygenic phototrophs use two photosystems (PSI and PSII) that constitute the Z-scheme and the associated generation of assimilatory power. Photosystems are multisubunit complexes in the thylakoid membrane and PSII absorbs and transforms light energy into chemical energy resulting in water splitting and oxygen evolution. PsbA (D1) and PsbD (D2) are the core subunits of PSII that exhibit photooxidoreductase activities and convert plastoquinone and water into plastoquinol (QH_2) and dioxygen (O_2). The Mn_4CaO_5 cluster is the oxygen evolution centre of PSII and is directly coordinated with multiple conserved residues of D1 and PsbC (CP43)-glutamic acid-354 (E354), further stabilised through second coordination spheres supported by conserved residues of D1, D2, and CP43 [1-3]. The tyrosine-161 (Y161) and histidine-190 (H190) residues of D1 work in tandem to transfer electrons to the reaction centre Chl *a* (P_{680}), wherein Y161 transfers electrons and H190 acts as a proton acceptor [4,5]. Charge separation involves the transfer of an electron from P_{680}, which then forms P_{680}^{+}, to primary acceptor (plastoquinone, Q) via an intermediary acceptor, pheophytin (Pheo *a*).

Amino acids residues surrounding the Mn_4CaO_5 cluster affect the PSII oxygen evolving capacity [6,7]. For example, a N181A/S mutation of the D1 protein results in slower O-O bond formation during water-splitting reaction in *Synechocystis* sp. PCC 6803 [8]. A D170A/S substitution of D1 poisons oxygen evolving capacity, while D170E mutation is complementary with little effect on the activity [9]. Additionally, the substitutions N87A/S, F117L, D170AES, and E189D in D1 results in impaired water-splitting activity and possibly reduced PSII stability [5].

 doi:10.20944/preprints202308.2051.v1

Cyanobacteria typically possess multiple *psbA* gene copies with different expression levels that mostly reflect varying environmental conditions [1,10-12]. For example, *Synechocystis* sp. PCC 6803 has three *psbA* genes with *psbA1* upregulated in high light, *psbA2* constitutively expressed [13], and *psbA3* expressed during low oxygen "microaerophilic" conditions. A general name of *psbA'* is given to "microaerophilic" *psbA* genes since other cyanobacteria have a comparable strategy [14].

Dark expression of sentinel *psbA* (belonging to the "rogue" D1 group) blocked oxygen-evolving PSII activity through an uncleavable C-terminus and altered amino acid residues surrounding the Mn_4CaO_5 cluster in nitrogen-fixing cyanobacterium *Cyanothece* [1,15,16]. Recently, a D1 variant was renamed "chlorophyll *f* synthase (ChlF)". It is a far-red light (FRL) induced paralog of D1 in Chl *f*-producing cyanobacteria [17]. The ChlF encoding gene participates in the far-red light-induced photoacclimation (FaRLiP) gene cluster and it is only transcribed under FRL conditions. It is unknown how ChlF catalyses the formation of chlorophyll *f* (Chl *f*) from Chl *a*, although molecular oxygen is required [18]. The ChlF-encoding gene from *Chroococcidiopsis thermalis* PCC 7203 (AFY86562) was used to replace the D1 subunit-encoding gene in the PSII complex of *Synechocystis* sp. PCC 6803 that resulted in up to ~0.1% Chl *f* of total chlorophyll when the transformant was grown photoheterotrophically with 5 mM glucose at a light intensity of 10–30 μmol photons m^{-2} s^{-1} [19]. ChlF is a D1 paralog that lacks many of the conserved amino acid residues surrounding the Mn_4CaO_5 cluster [1]. Those conserved amino acids in ChlF may play important roles in control of assembling an unconventional oxygen-evolving centre if ChlF substitutes for D1 in PSII complexes.

Chl *f* has a 2-formyl in the C2-position of Chl *a* responsible for the bulk red shifted absorption and possesses the most red-shifted absorption in chlorophylls [20]. Chl *f* enables cyanobacteria to utilize habitats in low white light (WL) and high FRL conditions [21-26]. The far-red light acclimation is also reported in endolithic cyanobacteria [22, 27,28]. Chl *f* is present in PSI and PSII when ChlF is heterologously expressed in *Synechocystis* sp. PCC 6803 and *Synechococcus* sp. PCC 7002 [19,29]. Chl *f* is detected in isolated PSI and PSII systems induced by FRL conditions in the following Chl *f*-producing cyanobacteria: *Chroococcidiopsis thermalis*, *Synechococcus* sp. PCC 7335, and *Halomicronema hongdechloris* [19,29-32] although there are quite few other cyanobacteria reported to produce Chl *f* [22-26]. Absorption spectra of naturally occurring Chl *f*-containing photosystems are more red-shifted than heterologously produced Chl *f*-containing PS complexes owing to a relatively higher Chl *f* content [29,32].

There are five *psbA* genes in the *H. hongdechloris* genome. In particular, *psbA2* (*XM38_018880*) codes for WL-D1 (or typical D1) protein in *H. hongdechloris* in WL conditions [33]. In turn, *psbA3* (*XM38_020870*) and *psbA4* (*XM38_037330*) are expressed in WL conditions but at a lower level than *psbA2* [33]. *H. hongdechloris* has paralogous genes encoding FRL-D2 (*XM38_010820*), FRL-CP47 (*XM38_010800*), FRL-CP43 (*XM38_010810*), FRL-PsbH (*XM38_010780*), FRL-PsbO (*XM38_010880*), and FRL-PsbV (*XM38_010890*) subunits of PSII in FRL grown cells. In addition, FRL-D1 (*XM38_010770*) and ChlF (*XM38_010900*) encoding genes in the FaRLiP gene cluster are up-regulated in FRL conditions [33].

The Mn_4CaO_5 cluster is the centre of water-splitting catalytic region and is directly coordinated with D1 and CP43 in PSII [34]. Cells grown in FRL conditions have a lower O_2-evolving rate than that of the cells grown under WL conditions [35]. ChlF from *H. hongdechloris* has over 70% conserved residues compared with typical D1 proteins. This supports an idea that ChlF may replace the WL-D1 subunit and exhibit a similar stability in the PSII complexes (33). A specific Q127 and D128 substitutions in ChlF (QD motif) is critical for activity and might be involved in binding the newly synthesised Chl *f* [19]. However, it is unclear whether these amino acid residues are directly involved in Chl *f* biosynthesis.

This report used published data on cyanobacterial PSII structure to characterize the functional motifs of ChlF from *H. hongdechloris* at the primary and 3D-structural modelling levels. As a whole, the new insights into the functional mechanisms of ChlF and Chl *f* biosynthesis should allow for a better understanding of the various functions of D1 paralogs.

 doi:10.20944/preprints202308.2051.v1

2. Materials and Methods

2.1. D1 protein sequence alignment

The FaRLiP gene cluster is used as a biomarker of Chl *f*-producing cyanobacteria. Eighteen cyanobacterial genomes possessing the FaRLiP cluster were selected and obtained from GenBank (NCBI) and Integrated Microbial Genomes of the DOE joint Genome Institute (Table S1). All putative ChlF and D1 sequences from 18 selected cyanobacterial genomes were retrieved with a total of 100 D1 paralogs. Identical copies were removed, and 83 sequences (Table S1) were used for sequence comparison. Sequence alignment was generated using Muscle in MEGA 11 and manually refined by predicting the PDB files from each D1 protein group using the SWISS-MODEL online service from ExPasy. The *H. hongdechloris* D2 protein was used as an outgroup.

2.2. The D1 sequence comparison

The D1 sequences were retrieved from cyanobacteria containing the FaRLiP gene clusters as described in Wang *et al.* 2022 [36] and then aligned based on the published D1 tree [11,12]. The subset of D1 homologs (including ChlF sequences) from 18 selected species of cyanobacteria containing the FaRLiP gene cluster were re-aligned with the typical D1 consensus sequence and refined manually according to conserved motifs and predicted secondary structures. The grouped D1 sequences were verified using neighbour-joining (NJ) phylogenetic analysis. The NJ distance tree was determined after 1,000 replications using the JTT (Jones, Taylor, and Thornton) model after the deletion of gaps [37].

2.3. *Structure modelling and comparison*

3D structural modelling was performed using Chimera version 1.14 [38], https://www.cgl.ucsf.edu/chimera/download.html. The PSII structural data from *Thermosynechococcus vestitus* BP-1 (also named as *Thermostichus vulcanus*) (PDB 5TIS and PDB 3WU2) (non Chl *f*-producing cyanobacteria) were used as templates to simulate structural models of D1 paralogs from *H. hongdechloris*. The following Uniprot data were predicted: A0A1Z3HIN9, *H. hongdechloris* ChlF (XM38_010900); A0A1Z3HJ62, *H. hongdechloris* FRL-D1 (XM38_010770); A0A1Z3HKW5, *H. hongdechloris* WL-D1 (XM38_018880); and P51765, *T. vulcanus* D1. Note that Uniprot P51765 has a R279P substitution compared with Uniprot P0A444 (D1 of *T. vulcanus*). All stimulated structure models were minimized and optimized after adding H-bonds and the protonation states of conserved charged amino acid residues, such as histidine (H) and glutamic acid (E). All predicted models were refined using Swissprot database (https://swissmodel.expasy.org) against the template file (5TIS.pdb). Swiss-model allows the production of a 3D model of heteromeric complexes [39], such as FRL-PSII complexes stimulated using PSII subunits from the FaRLiP cluster (FRL-PSII subunits). The individual 3D model of ChlF, FRL-D1, and WL-D1 of *H. hongdechloris* was used in place of D1 from *T. vulcanus* (PDB 5TIS). The heterodimers of D1/CP43/CP47/D2 from *H. hongdechloris* using WL-PSII and FRL-PSII subunits were predicted against the PDB 5TIS template.

Hydrogen atoms and hydrogen bonds are not observable in most crystal structures. However, many cofactors in PSII, such as Pheo *a* and plastoquinones Q_A and Q_B, interact with the D1 protein via hydrogen bonds (H-bonds). Therefore, hydrogen bonding is important to determine the physical structure parameters. The following criteria are needed to form H-bonds in a predicted protein structure: 1) donor atom−Acceptor atom <3.9 Å; 2) Hydrogen−Acceptor atom <2.5 Å; 3) donor atom−Hydrogen atom−Acceptor atom >90.0°; 4) adjacent atom to acceptor A'−Acceptor atom−Donor atom >90.0°; and 5) adjacent atom to acceptor A'−Acceptor atom−Hydrogen atom >90.0° as discussed in Torshin *et al.* [40] and McDonald and Thornton [41]. H-bond analysis was predicted and verified using the tools in Chimera.

Preprints (www.preprints.org) | NOT PEER-REVIEWED | Posted: 30 August 2023 doi:10.20944/preprints202308.2051.v1

3. Results

3.1. Alignment and phylogenetic relationship of D1 paralogs in Chl f-producing cyanobacteria

There are 19 published genomes containing the FaRLiP gene cluster. Eighteen of them are complete or incomplete whole genomes, and most are labelled as 'permanent drafts' (Table S1). D1 encoding genes and their paralogs were retrieved from GenBank (NCBI) and Integrated Microbial Genomes of the DOE joint Genome Institute and verified after BlastP comparison and annotation.

The D1 homologs can be divided into three main groups: WL-D1 (Typical D1), FRL-D1, and FRL-ChlF (Figure 1). According to protein alignments FRL-D1 proteins possess all essential conserved motifs of the D1 Protein and contribute to functional Chl *a*/*f*-binding PSII under FRL conditions including the high-affinity Mn-binding sites of D170 and E189 (Figure 2). The similar structures and conserved motifs among 18 FRL-D1 sequences can be defined as L40, G42, V43, S44, V47, T79, M114, Y119, P121, A122, L123, T154, S156, L172, M174, and L314, P315 (Figure 2).

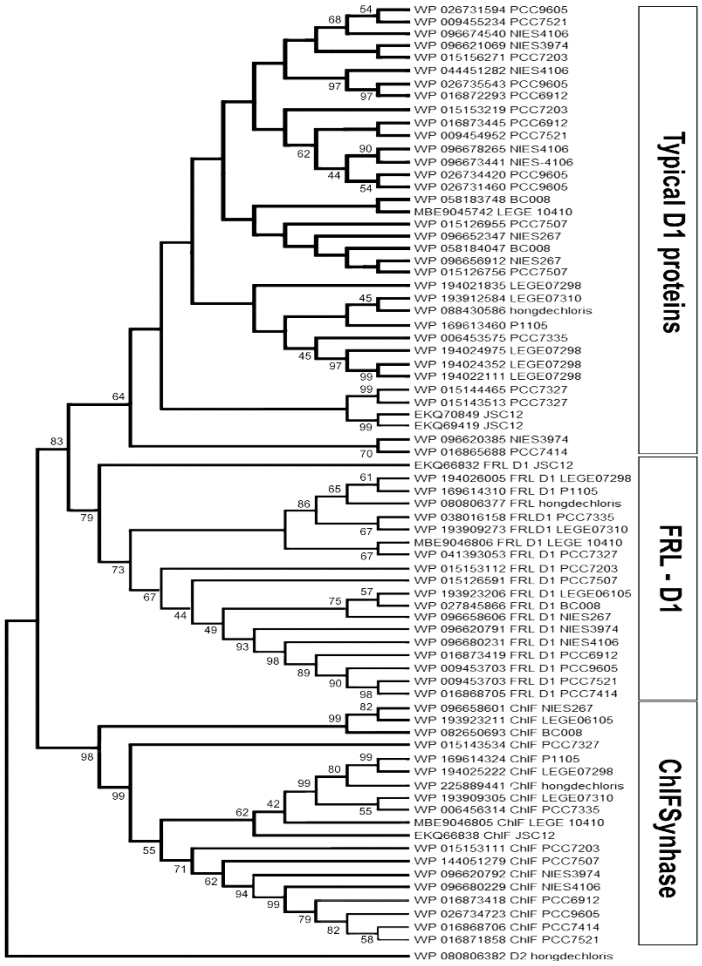

Figure 1. The neighbour-joining distance tree of D1 paralogs in Chl *f*-producing cyanobacteria. The distance tree was generated using the neighbour-joining (NJ) method in MEGA 11. *H. hongdechloris* D2 protein (WP080806382) was used as an outgroup. All sequence ID's and strain numbers used for the names and the sequence accession are listed in Table S1. The branch supports are calculated by 1,000 replications of NJ and were presented if the value was above 40%. Typical D1 groups include dominant D1 protein (WL-D1) of *H. hongdechloris* grown under white light conditions; FRL-D1 (far-red light D1), a group covering genes encoding D1 proteins in the FaRLiP cluster; and ChlF synthase, a new group of D1 paralogs that synthesize chlorophyll *f*.

Preprints (www.preprints.org) | NOT PEER-REVIEWED | Posted: 30 August 2023 doi:10.20944/preprints202308.2051.v1

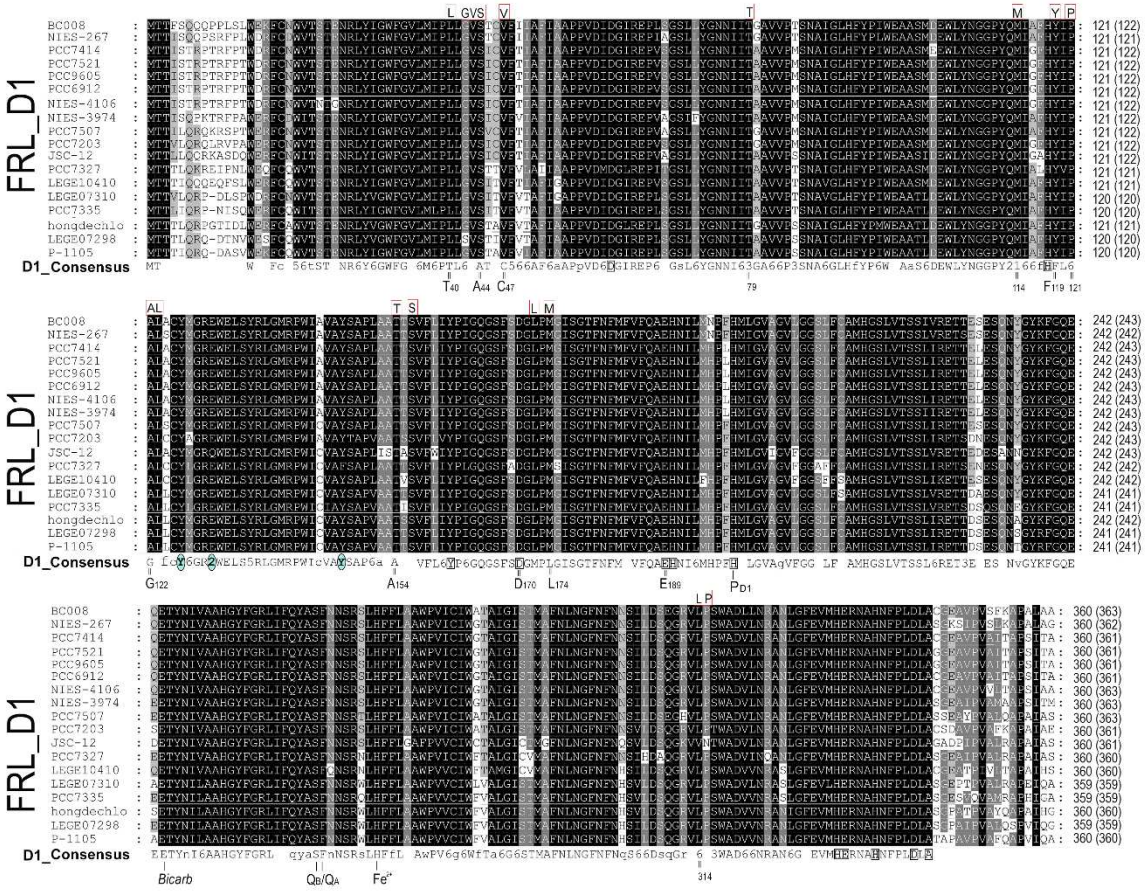

Figure 2. FRL-D1 protein sequence alignment supported by phylogenetic analysis in Figure 1. The specific conserved sites of FRL-D1 are highlighted by red framed boxes. The aligned sequence lengths are labelled as 'numbers (numbers)' at the end of each sequence. The numbers outside parentheses are aligned sequence lengths matching with the D1_consensus (unaligned gaps were removed), which is the number used in the models. The numbers inside parentheses represent the original length. The D1_consensus sequence surrounding the Mn_4CaO_5 cluster is highlighted in square boxes and bold fonts. The residues interacting with Pheo *a* in the D1_consensus sequence are highlighted with blue-colored circles. D1_consensus sequence was generated by Genedoc based on 50 typical D1 protein sequences. The conserved residues from 18 FRL-D1 sequences are highlighted with red-square boxes on the top of alignments and corresponding amino acid residues are numbered under D1_consensus sequence. The numbers in the D1_consensus represent the conservative substitutions: 2 = Q/E; 3 = S/T; 5 = MFY; 6 = F/I/L/M/V.

ChlF forms a distinct branch from FRL-D1 and other D1 groups (Figure 1). The similar residues among ChlF synthase sequences can be characterized as: L117, Q127, D128, S144, L145, F147, Q 252, and S285 (Figure 3), including the previously reported QD motif at sites 127 and 128 (Q152 and D153 of ChlF from *H. hongdechloris*) [19]. The sequence comparison confirmed that the substitution of H252Q is dominated in ChlF sequences, and only two cases of H252R substitutions were observed in *Pleurocapsa sp.* PCC 7327 and *Calothrix parasitica* NIES-267 (Figure 3). Interestingly, there is almost no overlap between the specific FRL-D1 motifs and ChlF sequences (Figure 2 and 3). ChlF demonstrated significant changes in the conserved residues surrounding the Mn_4CaO_5 cluster, although the most changed are not consistent in ChlF sequences as highlighted in Figure 3. For example, the conserved residue D170 in typical D1 sequence and it is A, S, and E in ChlF (Figure 3). Campbell *et al.* reported that Mn^{2+} was oxidized and stabilized as Mn^{4+} in a D170E mutant, resulting in a photoactivating PSII that produces oxidizing manganese (Mn^{4+}) but without O_2 evolution [42,43]. The substitutions N87A/S and D170AES are noticed in ChlF alignment and those changes in D1 impairs oxygen

Preprints (www.preprints.org) | NOT PEER-REVIEWED | Posted: 30 August 2023 doi:10.20944/preprints202308.2051.v1

evolution activities [5]. Thus, the replacement of D1 with the ChlF paralog may cause the loss of oxygen evolution.

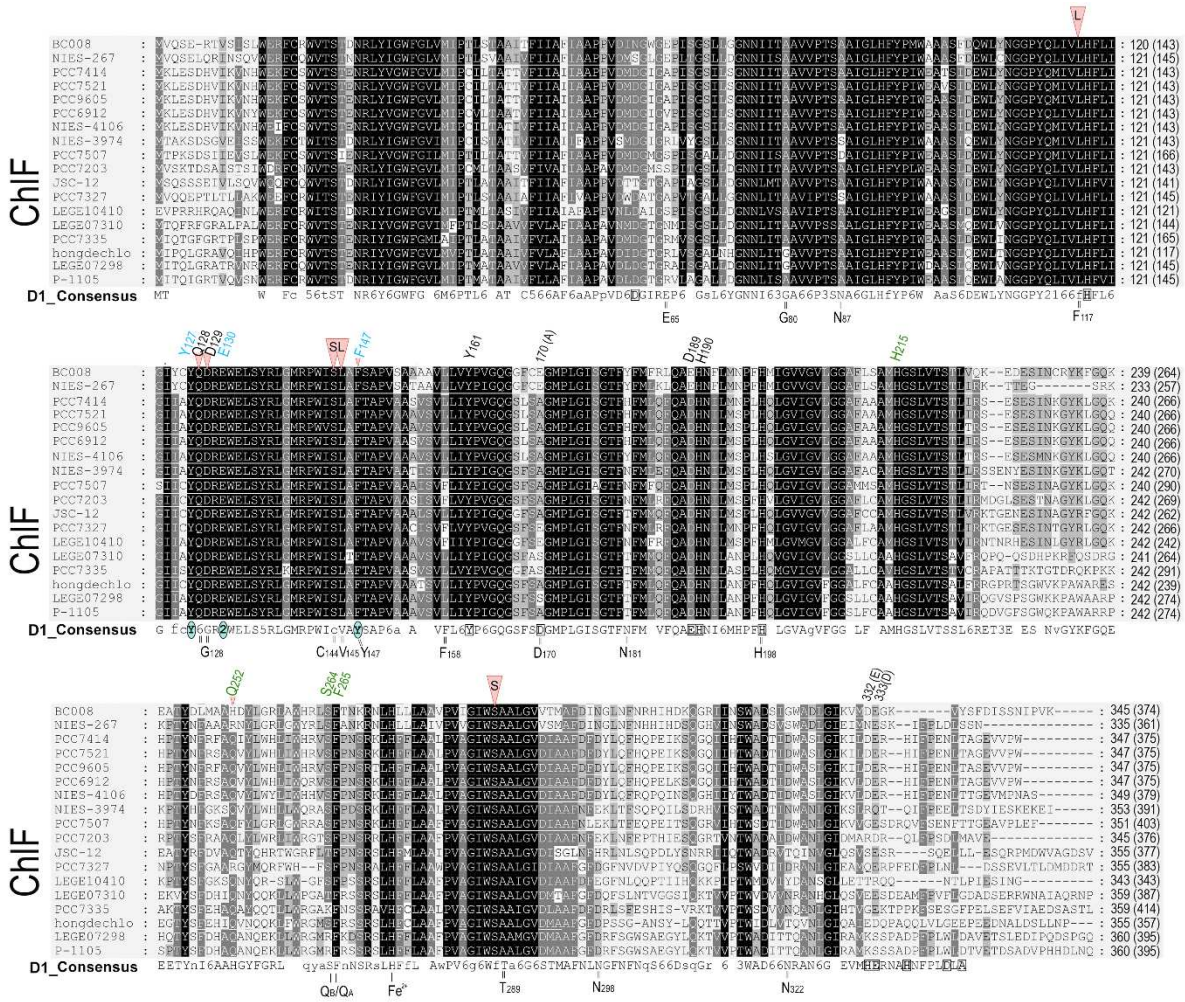

Figure 3. ChlF protein sequence alignment supported by phylogenetic analysis in Figure 1. The specific conserved sites of ChlF are highlighted by red triangles. The aligned sequence lengths are labelled as 'numbers (numbers)' at the end of each sequence. The numbers outside parentheses are aligned sequence length matching with D1_consensus (removed unaligned gaps), which is the number used in the models. The numbers inside parentheses represent the original length. The D1_consensus sequence surrounding the Mn_4CaO_5 cluster is highlighted with square boxes and bold fonts labelled in the D1_consensus sequences. The noticeable changed amino acid residues at the positions associated with the Mn_4CaO_5 cluster is labelled on the top of aligned ChlF sequences (Black coloured fonts). The residues interacting with Pheo *a* in the D1_consensus sequence are highlighted by blue coloured circles and their corresponding sites are labelled on the top of aligned ChlF sequences indicated as Blue-coloured fonts. The Amino acid residues surrounding Q_B site (as presented in Figure 5) are labelled on the top of aligned ChlF sequence indicated as Green-coloured fonts. D1_consensus sequences were generated by Genedoc based on 50 typical D1 protein sequences. The specific amino acid residues of ChlF are marked in pink triangle on the top of the alignment and corresponding amino acid residues are numbered under D1_consensus sequence. The numbers in the D1_consensus represent the conservative substitutions: 2 = Q/E; 3 = S/T; 5 = MFY; 6 = F/I/L/M/V. .

3.2. The modelling of D1 paralogs from H. hongdechloris

ChlF has over 70% conserved residues with D1 proteins. This allows for the generation of a reliable 3D model using structural templates of known PSII structures in cyanobacteria. PDB 3WU2 from *T. vulcanus* was initially used as the template for modelling ChlF. ChlF interaction with other

Preprints (www.preprints.org) | NOT PEER-REVIEWED | Posted: 30 August 2023 doi:10.20944/preprints202308.2051.v1

PSII subunits pertains to FRL-regulated structural reassembling subunits, especially FRL-D2 and FRL-CP43. The initial modelling trials without added H-atoms generated poor individual models of ChlF, FRL-D1, and WL-D1 (typical D1) since the estimated-overlap (3.5 Å) scores were well below 0.7 (Table S2). This score refers to the proportion of Cα atoms within 3.5 Å of the proposed modelling structures. The modelling of *H. hongdechloris* WL-D1 was relatively well matched against 3WU2-D1, including the positions of all functional motifs. Further, FRL-CP43 modelling was improved after adding H-atoms into the initial model (Table S2). The modelling results were further improved by excluding a certain number of amino acids at N- or C-termini and C-termini that do not align with the structural template. The estimated overlap scores were significantly improved to well above 0.7 after using the truncated sequences. The estimated overlap (3.5 Å) score of the truncated ChlF models was similar and above 0.9, with model 3 showing the highest score of 0.994 (Table S2).

3.3. Pheophytin a binding environment

Both FRL-D1 and ChlF have conserved E130 sites (Figures 2 and 3). The strength of hydrogen bond between this residue and Pheo *a* could be changed. The structures were further modelled by Swiss-model against the PDB 5TIS template from *T. vulcanus* [44]. The FRL-D1 model retained H-bonds with Pheo *a* and had a similar distance to the PDB 5TIS template, although the substitution of E130 (protonated at OE2) provided a stronger (shorter) H-bond than Q130 in the template (Figure 4). Hence, FRL-D1 demonstrated a comparable Pheo *a* binding profile to that in high-light acclimated cyanobacteria or plant PSII systems [45,46].

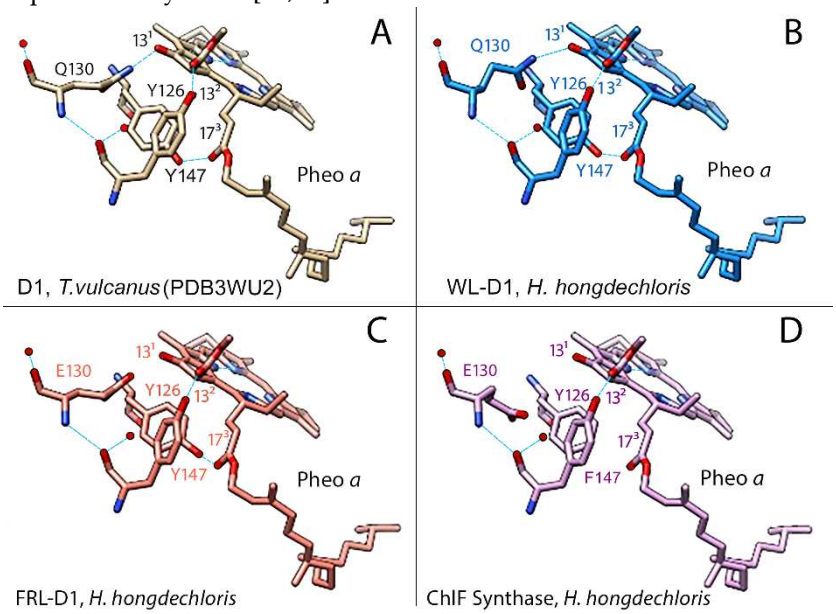

Figure 4. Modelling of the pheophytin *a* (Pheo *a*) binding region in WL-D1, FRL-D1, and ChlF of *H. hongdechloris*. *T. vulcanus* (PDB 3WU2) was used as a template. The amino acid positions known to form H-bonds (light blue lines) with Pheo *a*: Y126 (Tyr-O•••H•••O=C13^2-Pheo *a*); Q130/E130 (N-H or O-H) (Q-N•••H•••O=C13^1-Pheo *a*) or (E-O•••H•••O=C13^1-Pheo *a*), and Y147 (Tyr-O•••H•••O=C17^3-pheo *a*) are included to compare with the predicted H-bonds. **(a).** D1 of *T. vulcanus* PDB 3WU2 was used as a template for the modelled structure. **(b)**, **(c)**, and **(d)** represent models of the Pheo *a* binding region of WL-D1, FRL-D1, and ChlF synthase, respectively. Dark blue rods, nitrogen atoms; Red rods, oxygen atoms; Dotted light blue lines, H-bonds. **Note:** *FRL-D1 and ChlF synthase have E130, which may have H-bonds with 13^1-keto of pheo a, and these bonds might be stronger than Q130 (Table S3).*

ChlF modelling following the template placement of ligands generated H-bonds when E130 was selectively protonated at OE2; however, H-bonds were absent in non-protonated E130 and protonated E130-OE1 situations (Figure 4). ChlF retains the Y126 H-bond with C13^2 of Pheo *a* to provide a comparable H-bond distance to the template. But the Y147F substitution in ChlF results in

Preprints (www.preprints.org) | NOT PEER-REVIEWED | Posted: 30 August 2023 doi:10.20944/preprints202308.2051.v1

a loss of the H-bond, Y147-O•••H•••O2-C17^3-Pheo *a* (Figure 4, Figure S1, and Table S3). This contributes to the lessened interaction with Pheo *a*, although the impact of the missing H-bond with C17^3 Pheo *a* is unknown. The potential changed orientation of Pheo *a* due to loss of an H-bond at C17^3 Pheo *a* enhanced the strength of the H-bond with E130 in ChlF (Figure S1). Using flourescence relaxation measurement, Rappaport *et al.* observed acceleration of $S_2Q_A^-$ recombination process in Q130E mutant [45]. Thus, E130 in FRL-D1 and ChlF could decrease the recombination rate of $^1[P_{680}^+$/Pheo $a^-]$ to P^*_{680} in order to acclimate changed light environments.

3.4. Q_B binding environment

The typical D1 subunit has three H-bonds with two keto groups of Q_B: H215-N-H•••O=keto Q_B-O1, S264-O-H•••O=keto Q_B-O2, and F265N-H•••O=keto Q_B-O2. Additionally, S264 forms an H-bond with H252, H252-N-H•••O-S264 (Figure 5). Modelling of FRL-D1 and WL-D1 of *H. hongdechloris* simulated the H-bonds of H252-N-H•••O-S264 and the Q_B coupling environments were potentially unchanged (Figure 5). H252 protonation supports the protonation of Q_B to form Q_BH_2, an important electron transfer towards oxygen-evolving activities [47]. However, ChlF has a H252Q substitution that is known to affect electron transfer (Figure 5D). The lack of an H-bond between Q252 and S264 inhibits the putative protonation of Q_B and conversion of Q_BH_2 [2] and mutant of H252Q showed some rapid electron transfer from Q_A^- to Q_B [48]. The common substitution of H252Q (Figure 5D) implies that there is a more flexible structure in this region because H-bond formation should precede protonation to preserve some of the H-bonds supporting Q_B.

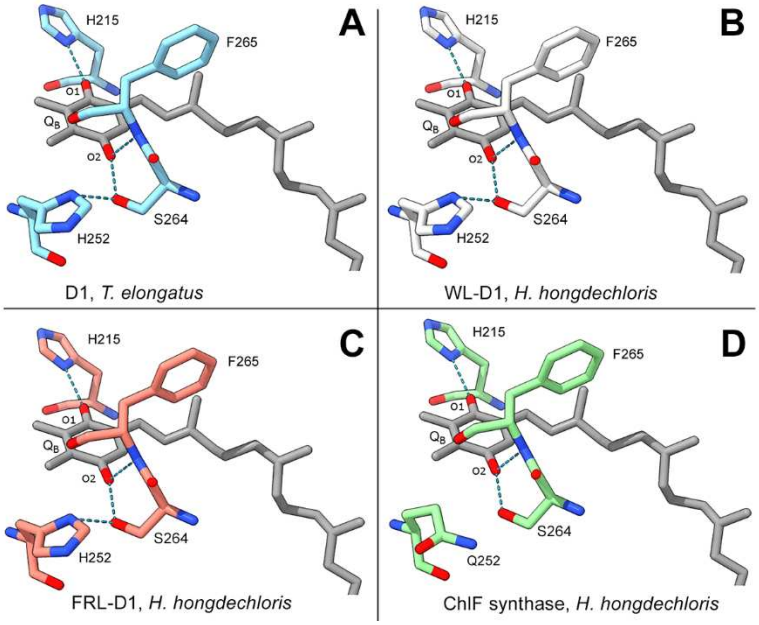

Figure 5. Modelled D1 paralogs surrounding Q_B. Modelling of WL-D1, FRL-D1, and ChlF of *H. hongdechloris* against the PDB 5TIS template from *T. vulcanus* (Young et al. 2016) was performed using Swissmodel. The conserved H-bonds of *T. vulcanus* D1 are shown as a positive control (a) to indicate modelling validity. **(b)**, *H. hongdechloris* WL-D1; **(c)**, *H. hongdechloris* FRL-D1; **(d)**, *H. hongdechloris* ChlF synthase. Q_B molecular bonds are in grey; residues from the *T. vulcanus* D1 template are in light blue; residues from *H. hongdechloris* WL-D1 are in white; residues from *H. hongdechloris* FRL-D1 are in orange; and residues from *H. hongdechloris* ChlF are in green; dark blue rods, nitrogen atoms; red rods, oxygen atoms; dotted light blue lines, H-bonds.

3.5. Putative Chl f-binding region of ChlF-PSII complexes

The specific QD motif in ChlF probably plays a biochemical role in the synthesis and binding of Chl *f*, which is at the position of CP43 binding to Chl *a* through the axial ligand, H441 [19]. ChlF was modelled with multiple rotamers to test the acceptable placement of Q127 or/and D128 substitutions.

Preprints (www.preprints.org) | NOT PEER-REVIEWED | Posted: 30 August 2023 doi:10.20944/preprints202308.2051.v1

There were clashes with the original placement of D128 and the Chl *a*/Chl *f* atoms. Position-c of the three putative spatial orientations of the formyl group of Chl *f* (designated C2-CHO$^{a/b/c}$) showed obvious clashes, while positions-a and -b only showed clashes with the C2 and C3 sub-groups of Chl *a* (Figure 6). Potential H-bonds were formed with D128-OE2 of ChlF after manually placing Chl *f* in the position of Chl *a* and confirmed after minimization and refinement of the model (Figure S2). However, no H-bonds were formed between the C2-formyl group of Chl *f* and protonated D128 at OE1 or when D128 was unprotonated (Figure S2). This was further supported in the minimized modelling structure of the ChlF-PSII complex. Therefore, protonated D128 at the OE2 position is the optimized situation in the modelled ChlF structure.

Further minimization steps included: 1) 2-formyl modification of Chl *a*-H441 of CP43 (CLA506.C); 2) H-bond formation, 3) protonation and H-atom addition of E130 OE2 and D128 OE2; 4) movement of Chl *f* into a favourable position for H-bond formation with D128 OE2; 5) the formation of a H-bond between D128 OE2 and Chl *f*. The refined and minimized structure proposed that the ideal placement occurred in rotamer model 7 if Chl *f* replaced Chl *a* in the region (Figure S2).

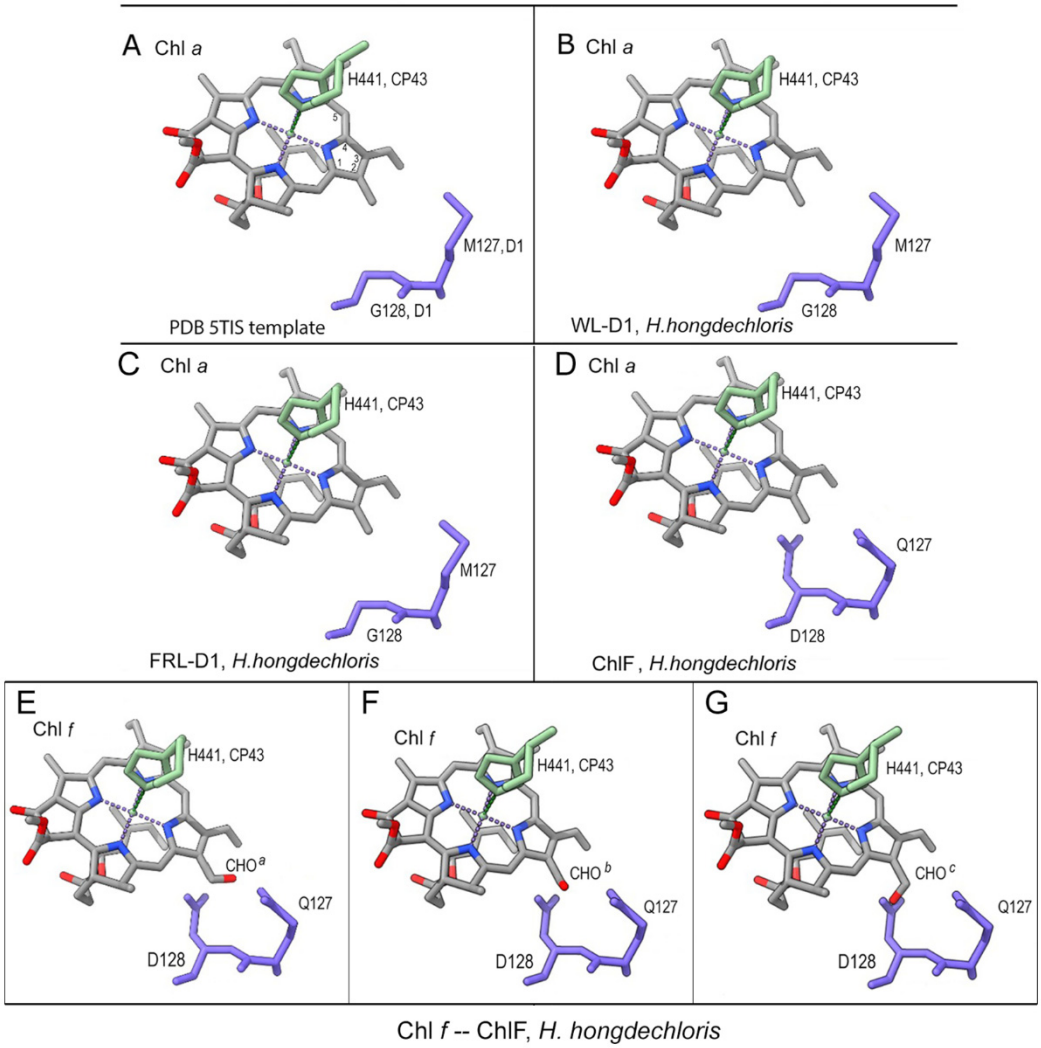

Figure 6. Position of the QD motif of ChlF compared with conserved MG residues from other D1 proteins. **(a)** Template 5TIS; **(b)** Modelled *H. hongdechloris* WL-D1; **(c)** Modelled *H. hongdechloris* FRL-D1; **(d)** Modelled *H. hongdechloris* ChlF. **(e-g),** Chl *a* was replaced with Chl *f* at the position of the modelled ChlF. The C2-CHO group of Chl *f* was shown at different orientations. E, position a; F, position b and G, position c of the oxygen atom of CHO. Chlorophyll molecular bonds are in grey; residues 127 and 128 of D1 and D1 paralogs are in purple-blue. The histidine (H441) of CP43 is in green. Dark blue rods, nitrogen atoms; red rods, oxygen atoms; dotted lines, H-bonds.

Preprints (www.preprints.org) | NOT PEER-REVIEWED | Posted: 30 August 2023 doi:10.20944/preprints202308.2051.v1

3.6. Mn_4CaO_5 cluster modelling

There is no consensus sequence for the Mn_4CaO_5 cluster following the alignment of ChlF sequences, despite some organisms retaining some of the typical amino acids (Figure 3). The significant changes of ChlF at the sites coordinating the Mn_4CaO_5 cluster (Figure 3) suggests that water splitting in a PSII-ChlF complex is impossible owing to the uncoupled Mn_4CaO_5 cluster. Multiple subunits of the *H. hongdechloris* PSII complexes were replaced with subunits of FRL-D1/D2/CP43/CP47 and/or ChlF/D2/CP43/CP47 and modelled using Swiss-Model.

The detailed environment surrounding the Mn_4CaO_5 cluster was demonstrated in Figure 7. The PSII-ChlF model showed conserved axial ligands H118 (D1), H198 (D1), H117 (D2), H197 (D2), together with H-bonds with Pheo *a*, Q_B, and the conserved Y161/H190 pair. And the presence of two conserved amino acid residues D/E189 (Mn1, Ca) of ChlF and E354 of CP43 (Mn2 and Mn3) suggests an Mn_4CaO_5 cluster may still be able to assemble or present in PSII-ChlF complex in an unconventional way (Figure 8). E189 provides a ligand to Mn in the metal cluster, but D189 from ChlF in *H. hongdechloris* showed no H-bond ligand to the metal cluster (Figure 8). D189 represents the conserved site in 16 ChlF sequences, except ChlF from *Mastigocoleus testarum* BC008 and *Calothrix parasitica* NIES-267, supporting dysfunctional oxygen evolution centre in PSII-ChlF complexes (Figure 3). The D1 mutant of E189D was reported to abolish water oxidation [4].

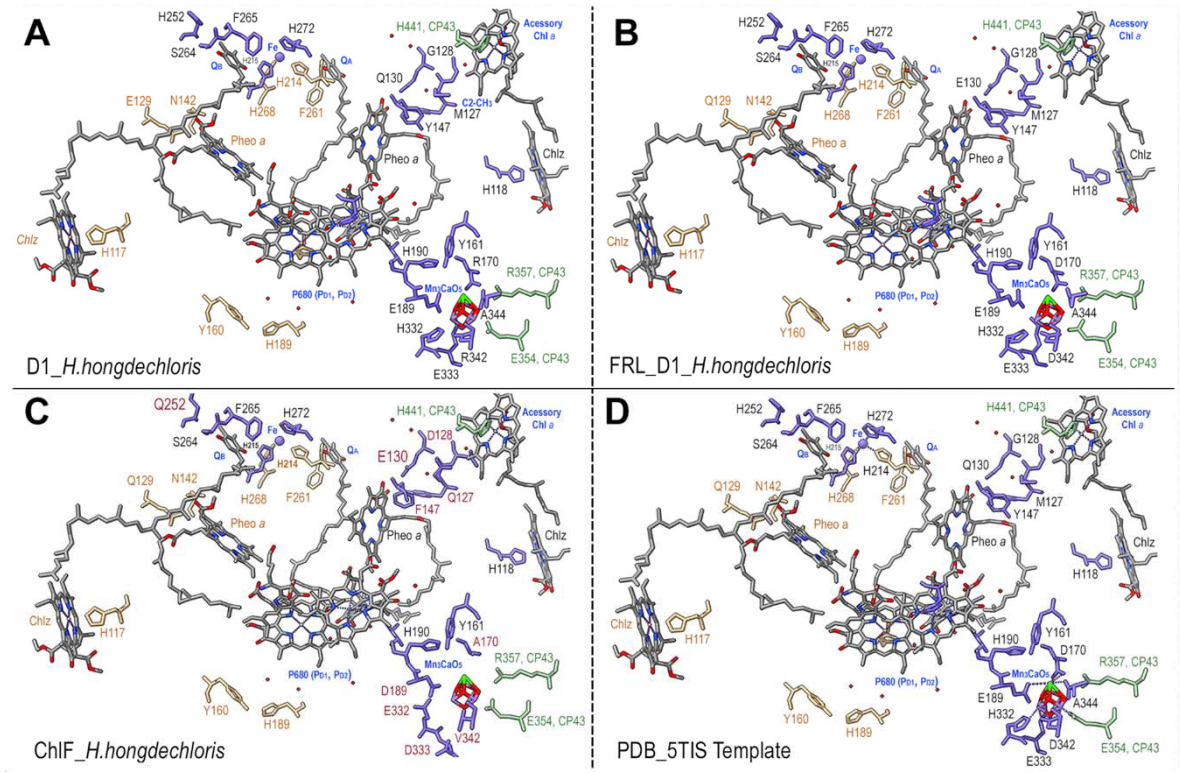

Figure 7. Models of PSII ligands involved in electron transport and water splitting. **(a)**. Typical PSII D1 of *H. hongdechloris* (WP088430586); **(b)**. *H. hongdechloris* FRL_D1 (WP080806377); **(c)**, *H. hongdechloris* ChlF (WP 225889441); **(d)**. PDB 5TIS template. The amino acids from CP43 are in green. The cofactors are in grey except for the Mn_4CaO_5 cluster. The unique ChlF residues are labelled in red. The D1 residues are in black fonts; the D2 residues are in brown fonts; the partial amino acid side-group bonds are in brown colors. Red rods, oxygen atoms (also represent the Mn in Mn_4CaO_5 cluster); dotted lines, H-bonds; dark green, Ca in Mn_4CaO_5 cluster.

Additionally, D170 involves the light-driven one electron oxidation of Mn^{2+} to Mn^{3+} and it is A170 from *H. hongdechloris* ChlF (Figure 8). The residues H332, E333, and D342, at the C-terminal of the typical D1 sequence are important for assembly Mn_4CaO_5 cluster and they are E332, D333 and V342 in *H. hongdechloris* ChlF sequence (Figure 3). According to the model, the ligands with Mn_4CaO_5 cluster are lacking in the ChlF sequence, indicating that these residue substitutions could lead to an

Preprints (www.preprints.org) | NOT PEER-REVIEWED | Posted: 30 August 2023 doi:10.20944/preprints202308.2051.v1

altered function and efficiency of PSII oxygen evolution. The E333D mutant in *Synechocystis* PCC 6803 showed no photosynthetic oxygen evolution and the H332E mutant appeared to induce the rapid charge recombination between Q_A^- and Yz^{ox} [49]. Therefore, the water splitting process is presumed deficient and ChlF probably has an alternative structure and function due to the several amino acid substitutions that are critical for coordinating the Mn_4CaO_5 cluster.

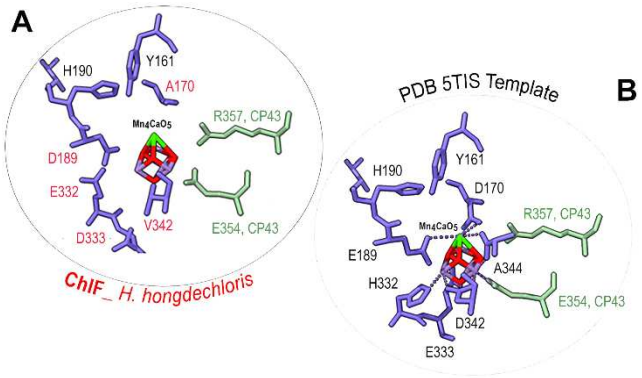

Figure 8. Detailed amino acid ligands surrounding the Mn_4CaO_5 cluster. **A**. Detailed model of ChlF from *H. hongdechloris* (WP 225889441); **B**. Structural details of the PDB 5TIS template. The conserved (black fonts) and different (red fonts) amino acids surrounding the Mn_4CaO_5 cluster. ChlF residues are in purple-blue. CP43 amino acids are in green. Red rods, the Mn in Mn_4CaO_5 cluster; dark green, Ca in Mn_4CaO_5 cluste; The dotted lines, H-bonds.

4. Discussion

The genes encoding FRL-D1 and ChlF are in the FaRLiP cluster under the same regulatory mechanism [33]. The different functions of D1 paralogs (FRL-D1 and ChlF) support the hypothesis of two different forms of PSII complexes assembled under FRL conditions. One of the substituted FRL-PSII of such complexes contains FRL-D1 and other FRL-PSII subunits. FRL-D1 proteins possess all essential conserved motifs of the D1 protein and agree well with published FRL-PSII cryo-EM structure [50], although the alignment of 18 FRL-D1 sequence showed variations at the positions of L124 with A/S/C and L206 with 3 species having F206 at the position (Figure 2). Presence of the critical residues coupling of oxygen evolving Mn_4CaO_5 cluster in FRL-D1 suggests a functional Chl *a/f*-binding PSII under FRL conditions as PSII-FRL-D1 complexes (Figure 2). Therefore, the FRL-PSII complex conducts PSII-performing charge separation and water-splitting reactions under FRL conditions, which is consistent with recent structure of PSII complexes acclimated to FRL conditions [50-52]. Meanwhile FRL-PSII complex (PSII-ChlF) containing the ChlF subunit instead of D1 proteins (FRL-D1 or WL-D1) plays a certain role in Chl *f* biosynthesis. PSII-ChlF contains the previously described QD motif [19] and presences of conserved L117, Q127, D128, S144, L145, F147, Q 252, and S285 in the 18 ChlF sequences. Six out of eight specific amino acid residues surrounding Mn4CaO5 are not shared with typical D1 and FRL-D1 although some changes are various between ChlF sequences (Figure 8). H332 from typical D1 changed as H332D, H332E, H332N, H332R, H332S, H332Q, and H332K in ChlF (Figure 3) and experimental data indicated most mutants abolished oxygen evolution capability and only mutants of H335S and H335Q gave 10-15% oxygen evolution rate [49]. The PSII-ChlF structural model supports a new function of ChlF although it shares >70% homology with D1.

4.1. Proposed uncoupled Mn_4CaO_5 cluster in PSII-ChlF complexes

The centre of oxygen evolving complex is the Mn_4CaO_5 cluster. It is stabilized with reaction centre proteins D1 and D2 and is surrounded by inner antenna proteins CP47 (near D2), and CP43 (near D1) [53]. Water-splitting proceeds in a multi-step process whereby the carefully positioned antenna chlorophylls of CP43 and CP47 transfer their excitation energy to reaction centre chlorophylls (P_{D1} and P_{D2}) of D1 and D2, respectively. Excited P_{680} donates electron to primary acceptor Pheo *a* which transmits it to Q_A and Q_B. Oxidized P_{680}^+ is reduced by an electron donated *via*

Y161 (Y_Z, D1) by the chemical splitting of water into oxygen. This occurs because the Mn_4CaO_5 cluster undergoes a series of redox reactions known as Kok's "oxygen clock" [half-reactions: $2H_2O \rightarrow 4H^+ + 4e^- + O_2$, and $2Q_B + 4H^+ + 4e^- \rightarrow 2Q_BH_2$]. Y_Z is an electron donor for P_{680}^+ of PSII and an electron carrier from the Mn_4CaO_5 cluster to the electron acceptor P_{680}^+.

ChlF synthase is a paralog of the reaction centre protein D1, however, structural modelling (Figure 3 and 7) confirmed the differences between ChlF and FRL-D1 and proposed an uncoupled Mn_4CaO_5 cluster in the PSII-ChlF complex. The proposed unconventional Mn_4CaO_5 cluster is supported by noticeable variations from ChlF sequences in the region of the 241-DEEE motif (Figure 3), the position to coordinating the bicarbonate in the typical D1 [1]. This is consistent with the hypothesis of "super-rogue" D1 proteins [1,11]. Additionally, N298 on D1 protein is required for oxygen evolution and mutants of N298D and N298E will impair oxygen evolving activity [54]. The substitution D298 and E298 occurs in 15 ChlF sequences (Figure 3).

P_{680}^+ is a powerful oxidant that facilitates the extraction of electrons from the Mn_4CaO_5 cluster via redox active Y_Z. Hence, reduction of P_{680}^+ might occur via cytochrome *b*559 and Chl *a*, or via Y_Z and Y_D in the absence of coordinated active Mn_4CaO_5 cluster. Electron donation to P_{680}^+ via Y_Z is still possible with the aid of Y_D at a higher pH environment; that is, Y_D can outcompete Y_Z in the reduction of P_{680}^+ at a higher pH [55]. The altered electron transfer in the PSII-ChlF complex may enable the reduction of P_{680}^+ by the oxygenation of Chl *a* at the C-2 position to produce Chl *f*.

4.2. The changed electron transfer pathways in dysfunctional PSII-ChlF complexes

ChlF has an unconventional coordinated Mn_4CaO_5 cluster (Figure 8). According to experimental data, the significant changes surrounding the Mn_4CaO_5 cluster could not support water oxidation and oxygen evolution even if it presents in PSII-ChlF complexes [4-7,49,54]. In additional, the changes at the D1 conserved sites N87, F117, D170, and E189 in ChlF (Figure 3) reduced PSII stability including the impaired water-splitting activities [5]. Another noticed changes around Pheo *a* including the feature substitution Q128D129 motif in ChlF (Figure 7). The conserved site of F147 in ChlF could shift the E_m(Pheo *a*/Pheo a^-) to more positive values and decrease the recombination rate of $^1[P_{680}^+$/Pheo *a*] to P^*_{680} [56]. However, ChlF has conserved Y_Z and Y_D together with H-bond partners H190 (D1) and H189 (D2) at similar modelled distances to that of D1. On the whole, this suggests that there is an altered electron transport efficiency from P_{680}^+ to primary and secondary acceptors. The presumed non-functional uncoupled Mn_4CaO_5 cluster in PSII-ChlF complexes suggests that Y_Z and Y_D supply the electrons required for the completion of redox reactions. Y160 of ChlF is conserved compared to other D1 sequences; however, this residue is not needed for the catalytic formation of Chl *f* [57]. Interestingly, the F147Y substitution in ChlF could cause the undelivered (or slower) electron at the level of Pheo *a*. Additionally, electron transfer within PSII is possible from a photooxidized reaction centre to Pheo *a*, Q_A, and Q_B. DCMU (3-(3,4-dichlorophenyl)-1,1-dimethylurea) is an inhibitor of the Q_B binding site and inhibits Chl *f* synthesis [57]. Therefore, the light-driven redox chemistry of PSII without the coupled Mn_4CaO_5 cluster would play an active role in Chl *f* biosynthesis.

PSII electron transfer follows the resonance energy migration within the light-harvesting antenna with the resulting excitation of the reaction centre primary donor (chlorophyll dimer P_{680}, or P_{D1} and P_{D2}) while the primary acceptor (Pheo *a*) reduces the primary quinone (Q_A). This causes a reduction of oxidized $P_{680}^{+\bullet}$ by Y_Z of D1 due to water oxidation by the coordinated Mn_4CaO_5 cluster. Impairment of the Mn_4CaO_5 cluster suggests that there is a longer-lived $P_{680}^{+\bullet}$ radical [58], and superoxide or H_2O_2 may be released as a long-lifetime free radical [59,60]. The expression of a ChlF encoding gene in a PSII-less mutant (D1/D2 double mutant) yielded Chl *f*, and its production was regulated by light-driven electron transfer [57]. Hence, a longer-lived $P_{680}^{+\bullet}$ radical is required for Chl *f* biosynthesis.

 doi:10.20944/preprints202308.2051.v1

4.3. Reaction mechanism of Chl f biosynthesis pathway

Oxidation of a methyl group to a formyl group is a difficult task because CH_3 is a chemically stable side-group. Free radical formation can be specifically involved [61-63]. Pheo *a* on the acceptor side of PSII may form singlet oxygen or hydroxyl free radical. Figure 4 suggests that the specific substituted residues of F147 in ChlF cause a loss of the H-bond at C17^3-Pheo *a* and a potential slower electron transfer rate, although there were no available experimental data, such as a constructed mutant of Y147F (Figure 4). The non-heme iron may also contribute to the formation of singlet oxygen or hydroxide radicals in the presence of light and aerobic conditions [64-67]. The inhibition of Chl *f* synthesis by DCMU implied that electron transports by primary and secondary acceptors Pheo *a*, Q_A, and Q_B were involved in the reaction chemistry [57]. As is known in PSII, the dominant pathway of charge recombination goes through the radical pair of [P_{680}^+/Pheo a^-] and an additional non-radiative pathway could proceed through repopulation of P^*_{680} from ^{1}[P_{680}^+/Pheo a^-], which was observed in D1 mutant Q130E in *Synechocystis* PCC 6803 [56]. We proposed the reaction scheme of Chl(Chlide) *f* synthesis from Chl(Chlide) *a* via free radical chemistry (Figure 9). Pheo *a* excitation in an oxygenated environment produces an anion radical ($D^{-\bullet}$) via singlet and triplet excited state coupled to electron donation by Chl *a*. The cation-radical of the Chl *a* methyl group is produced via deprotonation. This cation-radical reacted with dioxygen to form a peroxide further oxidized to superoxide or hydroxyl radical (Figure 9, step 4a) via reductants Pheo *a* (-610 mV) or Q_A^- (-80 mV) [68,69].

Peroxide radical can decompose to a hydroxymethyl-Chl derivative, and further react to form the formyl group in an unknown pathway (Figure 9, step 4b). Therefore, the altered electron pathway from P_{680}^+ to Pheo *a*, Q_A, and Q_B in the PSII-ChlF complex drives Chl *f* synthesis. The non-heme iron of PSII might not be involved in this oxygenation in the proposed mechanism; this differs from the biosynthetic mechanism of Chl *b* [70].

Chemical synthesis involving the oxidation of aromatic molecules with a methyl sidechain is often accomplished by free-radical chemistry using water as proton source under elevated temperatures; over-oxidation to the carboxylic acid is prevented by addition of a catalyst such as copper [71]. More recently, a radical-free mechanism was more specific for the synthesis of formyl groups [72]. ChlF has a likely impaired oxygen evolving cluster; therefore, there is an increased potential of light-induced photoinhibition (even under low visible light) [73]. Two important photoinhibition sites in PSII include charge separation between P_{680}^+ and Q_A^-, and electron transfer from Y_Z to P_{680}^+ [74]. Photoinhibition can cause carotenoid and chlorophyll radicals (from photopigments adjacent to P_{680} and accessory Chls) following the loss of Y_Z and Y_D radicals [75]. Accessory Chls and carotenoids in PSII have been proven to represent sites of photoinhibition damage following a hydroxylamine treatment [76]. It is unclear if ChlF is degraded during photoinhibition since detailed studies are unavailable. The A345, S345, or F345 substitutions in the functional domain of D1 resulted in comparable hydrolysis rates following carboxyl-terminal processing protease (CtpA), while G345 and V345 substitutions showed lower hydrolysis rates [77]. However, the P345 substitution resulted in complete inhibition [77].

Preprints (www.preprints.org) | NOT PEER-REVIEWED | Posted: 30 August 2023 doi:10.20944/preprints202308.2051.v1

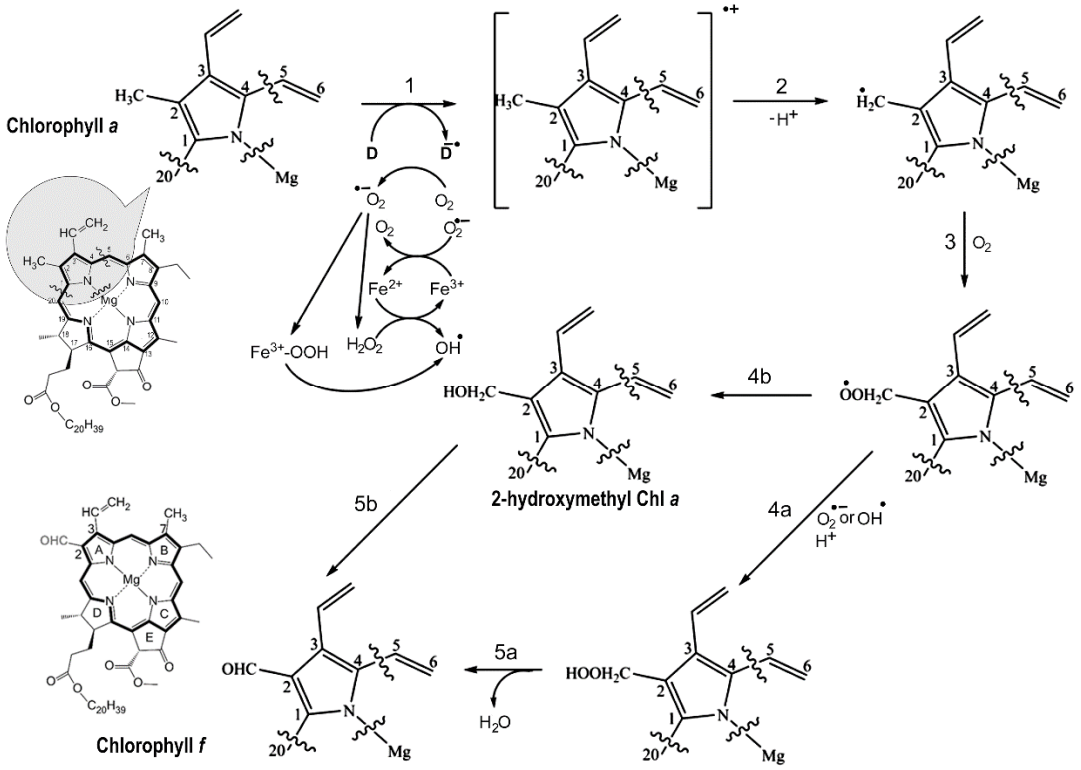

Figure 9. Proposed chlorophyll *f* biosynthesis reaction schemes. The proposed free-radical reaction schemes of chlorophyll *f* synthesis from chlorophyll *a* wherein the C2 methyl group in Chl *a* is transformed into a formyl group in Chl *f*. The first step involves the formation of an anion radical (D-•) that might be the overexcited Pheo *a* in an oxygenated aqueous environment, or a light-activated radical species through the coupled electron donation by the Chl *a* molecule. Deprotonation forms the radical methyl cation of the Chl *a* substrate (Step 2), followed by reaction with oxygen to generate a peroxo radical (Step 3) that reacts with a superoxide or hydroxy radical (Step 4a) produced through the reduction of oxygen by light activated reductants, such as Pheo *a* (-610 mV) and Q_A (-80 mV). This formed the unstable hydroperoxymethyl Chl that was further hydrolyzed to the formyl group (Chl *f*). Alternatively, the peroxo radical may decompose to the hydroxymethyl Chl derivative (Step 4b) that further reacts in an unknown pathway to form the formyl group (Step 5b). The partial structure of chlorophylls showed the side-group containing the C2-methyl of Chl *a* (shaded region).

ChlF has two unique S motifs in addition to the QD motif (Figure 3) that are likely hydrolysis sites with potentially lower hydrolysis rates. The H-bond between Y_Z and H190 of ChlF is potentially retained, although there may be H-bonds with other amino acids when the Mn_4CaO_5 cluster is depleted or uncoupled. Hence, electron transfer from Y_Z to P_{680}^+ is possible without the coupled functional Mn_4CaO_5 cluster although it could be slower [2,78,79]. Therefore, a long-lived P_{680}^+ may exist in PSII-ChlF complex that functions as a powerful oxidant with a redox potential of approximately 1.13 mV [78].

Replacement of an MG motif in D1 to a unique QD motif in ChlF facilitates the production of Chl *f in vivo*. This suggests that the QD motif is the most probable active site of the enzyme, although it is unknown whether close proximity of D128 is critical [19]. Further work is required to determine whether photoinhibition (or free radical formation) in the PSII-ChlF complex in fact catalyzes Chl *f* production.

Supplementary Materials: The following supporting information can be downloaded at the website of this paper posted on Preprints.org, **Figure S1**: Detailed H-bonds surrounding cofactor Pheo *a* in the models; **Figure S2:** Simulated models of ChlF containing chlorophyll *f* at different rotamers of protonated D128; **Table S1**: Genetic information of selected 19 cyanobacteria; **Table S2:** Modelling results of ChlF synthase, FRL-D1, WL-

D1, FRL-CP43L, and WL-CP43 of *H. hongdechloris* against template PDB3WU2 with or without the inclusion of H atoms included during modelling; **Table S3:** H-bonding distances (Å) between pheophytin 13^1-keto and 13^2-keto groups and D1 of *T. vulcanus* (PDB3WU2), WL-D1, FRL-D1, and ChlF synthase from *H. hongdechloris* by the amino acids Q130/E130, Y126, and Y147 or F147, respectively.

Author Contributions: MC coordinated the project, involving designed research, conduced data analysis, and wrote the manuscript. AS performed PSII modelling and assisted with the writing. FW performed phylogenetic analysis and secondary structure alignments.

Funding: This research was partially supported by Australia Research Council Centre of Excellence for Translational Photosynthesis (CE140100015) and Discovery Project DP210102187.

Conflicts of Interest: The authors have no conflicts of interest to declare that are relevant to the content of this article.

References

1. Cardona T, Murray JW, Rutherford AW (2015) Origin and evolution of water oxidation before the Last Common Ancestor of the Cyanobacteria. Mol Biol Evol 32:1310-1328. https://doi.org/10.1093/molbev/msv024
2. Umena Y, Kawakami K, Shen J-R, Kamiya N (2011) Crystal structure of oxygen-evolving photosystem II at a resolution of 1.9 A. Nature 473:55-60. https://doi.org/10.1038/nature09913
3. Service RJ, Yano J, McConnell I, Hwang HJ, Niks D, Hille R, *et al.* (2011) Participation of glutamate-354 of the CP43 polypeptide in the ligation of manganese and the binding of substrate water in Photosystem II. Biochemistry 50:63-81. https://doi.org/10.1021/bi1015937
4. Chu HA, Nguyen AP, Debus RJ (1995) Amino acid residues that influence the binding of manganese or calcium to photosystem II. 1. The lumenal interhelical domains of the D1 polypeptide. Biochemistry 34:5839-5858. https://doi.org/10.1021/bi00017a016
5. Diner BA (2001) Amino acid residues involved in the coordination and assembly of the manganese cluster of photosystem II. Proton-coupled electron transport of the redox-active tyrosines and its relationship to water oxidation. Biochim Biophys Acta Bioenerg 1503:147-163. https://doi.org/10.1016/s0005-2728(00)00220-6
6. Dilbeck PL, Bao H, Neveu CL, Burnap RL (2013) Perturbing the water cavity surrounding the manganese cluster by mutating the residue D1-valine 185 has a strong effect on the water oxidation mechanism of Photosystem II. Biochemistry 52:6824-6833. https://doi.org/10.1021/bi400930g
7. Service RJ, Hillier W, Debus RJ (2014) Network of hydrogen bonds near the oxygen-evolving Mn4CaO5 cluster of Photosystem II probed with FTIR difference spectroscopy. Biochemistry 53:1001-1017. https://doi.org/10.1021/bi401450y
8. Pokhrel R, Debus RJ, Brudvig GW (2015) Probing the effect of mutations of asparagine 181 in the D1 subunit of Photosystem II. Biochemistry 54:1663-1672. https://doi.org/10.1021/bi501468h
9. Nixon PJ, Diner BA (1992) Aspartate 170 of the photosystem II reaction center polypeptide D1 is involved in the assembly of the oxygen-evolving manganese cluster. Biochemistry 31:942-948. https://doi.org/10.1021/bi00118a041
10. Kiss E, Kós PB, Chen M, Vass I (2012) A unique regulation of the expression of the *psbA, psbD*, and *psbE* genes, encoding the D1, D2 and cytochrome b559 subunits of the Photosystem II complex in the chlorophyll *d* containing cyanobacterium *Acaryochloris marina*. Biochim Biophys Acta Bioenerg 1817:1083-94. https://doi.org/10.1016/j.bbabio.2012.04.010
11. Murray JW (2012) Sequence variation at the oxygen-evolving centre of photosystem II: a new class of 'rogue' cyanobacterial D1 proteins. Photosyn Res 110:177-184. https://doi.org/10.1007/s11120-011-9714-5.
12. Sheridan KJ, Dunca, EJ, Eaton-Rye JJ, Summerfield TC (2020). The diversity and distribution of D1 proteins in cyanobacteria. Photosynth Res 145, 111–128. https://doi.org/10.1007/s11120-020-00762-7
13. Mohamed A, Eriksson J, Osiewacz HD, Jansson C (1993) Differential expression of the *psbA* genes in the cyanobacterium *Synechocystis* 6803. Mol Gen Genet 238:161-168. https://doi.org/10.1007/BF00279543
14. Sicora CI, Ho FM, Salminen T, Styring S, Aro E-M (2009) Transcription of a "silent" cyanobacterial *psbA* gene is induced by microaerobic conditions. Biochim Biophys Acta Bioenerg 1787:105-112. https://doi.org/10.1016/j.bbabio.2008.12.002
15. Zhang X, Sherman LA (2012) Alternate copies of D1 are used by cyanobacteria under different environmental conditions. Photosyn Res 114:133-135. https://doi.org/10.1007/s11120-012-9783-0
16. Wegener KM, Nagarajan A, Pakrasi HB (2015) An atypical *psbA* Gene Encodes a sentinel D1 protein to form a physiologically relevant inactive Photosystem II complex in cyanobacteria. J Biol Chem 290:3764-3774. https://doi.org/10.1074/jbc.M114.604124
17. Ho M-Y, Shen G, Canniffe DP, Zhao C, Bryant DA (2016) Light-dependent chlorophyll *f* synthase is a highly divergent paralog of PsbA of photosystem II. Science 353:886. https://doi.org/10.1126/science.aaf9178

18. Garg H, Loughlin PC, Willows RD, Chen M (2017) The C21-formyl group in chlorophyll *f* originates from molecular oxygen. J Biol Chem 292:19279-19289. https://doi.org/10.1074/jbc.M117.814756
19. Trinugroho JP, Bečková M, Shao S, Yu J, Zhao Z, Murray J, *et al.* (2020) Chlorophyll *f* synthesis by a super-rogue photosystem II complex. Nat Plants 6:238-244. https://doi.org/10.1038/s41477-020-0616-4
20. Chen M, Schliep M, Willows RD, Cai ZL, Neilan BA, Scheer H (2010) A red-shifted chlorophyll. Science 329:1318-1319. https://doi.org/10.1126/science.1191127
21. Chen M, Li Y, Birch D, Willows RD (2012) A cyanobacterium that contains chlorophyll *f* – a red-absorbing photopigment. FEBS Lett 586:3249-3254. https://doi.org/10.1016/j.febslet.2012.06.045
22. Zhang ZC, Li ZK, Yin YC, Li Y, Jia Y, Chen M, *et al.* (2019) Widespread occurrence and unexpected diversity of red-shifted chlorophyll producing cyanobacteria in humid subtropical forest ecosystems. Environ Microbiol 21:1497-1510. https://doi.org/10.1111/1462-2920.1458215.
23. Gan F, Shen G, Bryant DA (2015) Occurrence of far-red light photoacclimation (FaRLiP) in diverse cyanobacteria. Life. 5: 4-24. https://doi.org/10.3390/life5010004.
24. Averina SG, Velichko N, Senatskaya E, Pinevich A (2018) Far-red photoadaptations in aquatic cyanobacteria. Hydrobiologia. 813:1-17. https://doi.org/10.1007/s10750-018-3519-x.
25. Gómez-Lojero C, Leyva-Castillo LE, Herrera-Salgado P, Barrero-Rojas J, Rios-Castro E, Gutiérrez-Cirlos EB (2018) *Leptolyngbya* CCM 4, a cyanobacterium with far-red photoacclimation from Cuatro Ciénegas Basin, México. Photosynthetica. 56: 342-353. https://doi.org/10.1007/s11099-018-0774-z
26. Averina SG, Velichko NV, Pinevich AA, Senatskaya EV, Pinevich AV (2019) Non-a chlorophylls in cyanobacteria. Photosynthetica. 57:1109-1118. https://doi.org/10.32615/ps.2019.130
27. Billi D, Napoli A, Mosca C, Fagliarone C, de Carolis R, Balbi A, Scanu M, Selinger VM, Antonaru LA, Nürnberg DJ (2022) Identification of far-red light acclimation in an endolithic *Chroococcidiopsis* strain and associated genomic features: Implications for oxygenic photosynthesis on exoplanets. Front. Microbiol. 13:933404. https://doi.org/10.3389/fmicb.2022.933404.
28. Murray B, Ertekin E, Dailey M, Soulier NT, Shen G, Bryant DA, Perez-Fernandez C, DiRuggiero J (2022) Adaptation of cyanobacteria to the endolithic light spectrum in hyper-arid deserts. Microorganisms. 10: 1198. https://doi.org/10.3390/microorganisms10061198.
29. Tros M, Bersanini L, Shen G, Ho M-Y, van Stokkum IHM, Bryant DA, *et al.* (2020) Harvesting far-red light: Functional integration of chlorophyll *f* into Photosystem I complexes of *Synechococcus* sp. PCC 7002. Biochim Biophys Acta Bioenerg 1861:148206. https://doi.org/10.1016/j.bbabio.2020.148206
30. Nürnberg DJ, Morton J, Santabarbara S, Telfer A, Joliot P, Antonaru LA, *et al.* (2018) Photochemistry beyond the red limit in chlorophyll *f*–containing photosystems. Science 360:1210-1213. https://doi.org/10.1126/science.aar8313
31. Kurashov V, Ho M-Y, Shen G, Piedl K, Laremore TN, Bryant DA, *et al.* (2019) Energy transfer from chlorophyll *f* to the trapping center in naturally occurring and engineered Photosystem I complexes. Photosyn Res 141:151-163. https://doi.org/10.1007/s11120-019-00616-x
32. Li Y, Vella N, Chen M (2018) Characterization of isolated photosystem I from *Halomicronema hongdechloris*, a chlorophyll *f*-producing cyanobacterium. Photosynthetica 56:306-315. https://doi.org/10.1007/s11099-018-0776-x
33. Chen M, Hernández-Prieto MA, Loughlin PC, Li Y, Willows RD (2019) Genome and proteome of the chlorophyll *f*-producing cyanobacterium *Halomicronema hongdechloris*: adaptative proteomic shifts under different light conditions. BMC Genom 20:207. https://doi.org/10.1186/s12864-019-5587-3
34. Junge W (2019) Oxygenic photosynthesis: history, status and perspective. Q Rev Biophys 52:e1. https://doi.org/10.1017/S0033583518000112
35. Li Y, Lin Y, Loughlin P, Chen M (2014) Optimization and effects of different culture conditions on growth of *Halomicronema hongdechloris* – a filamentous cyanobacterium containing chlorophyll *f*. Front Plant Sci 5:67. https://doi.org/10.3389/fpls.2014.00067
36. Wang F, Chen M (2022) Chromatic acclimation processes and their relationships with phycobiliprotein complexes. Microorganisms 10:1562. https://doi.org/10.3390/microorganisms10081562
37. Jones DT, Taylor WR, Thornton JM (1992) The rapid generation of mutation data matrices from protein sequences. Comput Appl Biosci 8:275-82. https://doi.org/10.1093/bioinformatics/8.3.275
38. Kelley LA, Mezulis S, Yates CM, Wass MN, Sternberg MJE (2015) The Phyre2 web portal for protein modeling, prediction and analysis. Nat Protoc 10:845-858. https://doi.org/10.1038/nprot.2015.053
39. Waterhouse A, Bertoni M, Bienert S, Studer G, Tauriello G, Gumienny R, *et al.* (2018) SWISS-MODEL: homology modelling of protein structures and complexes. Nucleic Acids Res 46:W296-W303. https://doi.org/10.1093/nar/gky427
40. Torshin IY, Weber IT, Harrison RW (2002) Geometric criteria of hydrogen bonds in proteins and identification of `bifurcated' hydrogen bonds. Protein Eng Des Sel 15:359-363. https://doi.org/10.1093/protein/15.5.359
41. McDonald IK, Thornton JM (1994) Satisfying hydrogen bonding potential in proteins. J Mol Biol 238:777-793. https://doi.org/10.1006/jmbi.1994.1334

42. Campbell KA, Force DA, Nixon PJ, Dole F, Diner BA, Britt RD (2000) Dual-mode EPR detects the initial intermediate in photo assembly of the photosystem II Mn cluster: The influence of amino acid residue 170 of the D1 polypeptide on Mn coordination. *J Am Chem Soc.* 122:3754–3761. https://doi.org/10.1021/ja000142t
43. Johnson JE, Webb SM, Thomas K, Ono S, Kirschvink JL, Fischer WW (2013) Manganese-oxidizing photosynthesis before the rise of cyanobacteria. Proc Natl Acad Sci U S A. 110:11238-43. doi: 10.1073/pnas.1305530110.
44. Young ID, Ibrahim M, Chatterjee R, Gul S, Fuller FD, Koroidov S, *et al.* (2016) Structure of photosystem II and substrate binding at room temperature. Nature 540:453-457. https://doi.org/10.1038/nature20161
45. Rappaport F, Guergova-Kuras M, Nixon PJ, Diner BA, Lavergne J (2002) Kinetics and pathways of charge recombination in photosystem II. Biochemistry 41:8518-8527. https://doi.org/10.1021/bi025725p
46. Dorlet P, Xiong L, Sayre RT, Un S (2001) High field EPR study of the pheophytin anion radical in wild type and D1-E130 mutants of Photosystem II in *Chlamydomonas reinhardtii*. J Biol Chem 276:22313-22316. https://doi.org/10.1074/jbc.M102475200
47. Lupínková L, Metz JG, Diner BA, Vass I, Komenda J (2002) Histidine residue 252 of the Photosystem II D1 polypeptide is involved in a light-induced cross-linking of the polypeptide with the α subunit of cytochrome *b*-559: study of a site-directed mutant of *Synechocystis* PCC 6803. Biochim Biophys Acta Bioenerg 1554:192-201. https://doi.org/10.1016/s0005-2728(02)00243-8
48. Petrouleas V, Crofts A (2005) The iron -quinone acceptor complex In: Wydrzynski TJ, Satoh K editors Photosystem II: the light-driven water:plastoquinone oxidoreductase. Dordrecht: Springer. P177-206.
49. Chu HA, Nguyen AP, Debus RJ (1995) Amino acid residues that influence the binding of manganese or calcium to photosystem II. 2. The carboxy-terminal domain of the D1 polypeptide. Biochemistry. 34:5859-82. doi: 10.1021/bi00017a017.
50. Gisriel CJ, Shen G, Ho MY, Kurashov V, Flesher DA, Wang J, Armstrong WH, Golbeck JH, Gunner MR, Vinyard DJ, Debus RJ, Brudvig GW, Bryant DA (2022) Structure of a monomeric photosystem II core complex from a cyanobacterium acclimated to far-red light reveals the functions of chlorophylls d and f. J Biol Chem. 298:101424. doi: 10.1016/j.jbc.2021.101424.
51. Gisriel CJ, Cardona T, Bryant DA, Brudvig GW (2022) Molecular Evolution of Far-Red Light-Acclimated Photosystem II. Microorganisms. 10(7):1270. https://doi.org/10.3390/microorganisms10071270.
52. Gisriel CJ, Shen G, Flesher DA, Kurashov V, Golbeck JH, Brudvig GW, Amin M, Bryant DA (2023) Structure of a dimeric photosystem II complex from a cyanobacterium acclimated to far-red light. J Biol Chem. 299:102815. doi: 10.1016/j.jbc.2022.102815.
53. Renger G, Renger T (2008) Photosystem II: The machinery of photosynthetic water splitting. Photosyn Res 98:53-80. https://doi.org/10.1007/s11120-008-9345-7
54. Kuroda H, Kodama N, Sun XY, Ozawa S, Takahashi Y (2014) Requirement for Asn298 on D1 protein for oxygen evolution: analyses by exhaustive amino acid substitution in the green alga Chlamydomonas reinhardtii. Plant Cell Physiol. 55:1266-75. doi: 10.1093/pcp/pcu073.
55. Faller P, Rutherford AW, Debus RJ (2002) Tyrosine D oxidation at cryogenic temperature in photosystem II. Biochemistry 41: 12914-12920. https://doi.org/10.1021/bi026588z
56. Cser K, Vass I (2007) Radiative and non-radiative charge recombination pathways in Photosystem II studied by thermoluminescence and chlorophyll fluorescence in the cyanobacterium *Synechocystis* 6803. Biochim Biophys Acta. 1767:233-43. doi: 10.1016/j.bbabio.2007.01.022.
57. Shen G, Canniffe DP, Ho M-Y, Kurashov V, van der Est A, Golbeck JH, *et al.* (2019) Characterization of chlorophyll *f* synthase heterologously produced in *Synechococcus* sp. PCC 7002. Photosyn. Res 140:77-92. https://doi.org/10.1007/s11120-018-00610-9
58. Hakala M, Tuominen I, Keränen M, Tyystjärvi T, Tyystjärvi E (2005) Evidence for the role of the oxygen-evolving manganese complex in photoinhibition of Photosystem II. Biochim Biophys Acta Bioenerg 1706:68-80. https://doi.org/10.1016/j.bbabio.2004.09.001
59. Wood P M (1988) The potential diagram for oxygen at pH 7. Biochemical Journal 253:287-289. https://doi.org/ 10.1042/bj2530287
60. Vass I (2012) Molecular mechanisms of photodamage in the Photosystem II complex. Biochim Biophys Acta Bioenerg 1817:209-217. https://doi.org/10.1016/j.bbabio.2011.04.014
61. Julliard M, Galadi A, Chanon M (1990) Oxidation of methyl aromatic compounds by redox photosensitization. J Photochem Photobiol A: Chemistry 54:79-90. https://doi.org/10.1016/1010-6030(90)87011-Y
62. Kiener A (1992) Enzymatic oxidation of methyl groups on aromatic heterocycles: a versatile method for the preparation of heteroaromatic carboxylic acids. Angew Chem Int Ed Engl 31:774-775. https://doi.org/10.1002/anie.199207741
63. Bienvenu C, Wagner JR, Cadet J (1996) Photosensitized oxidation of 5-methyl-2'-deoxycytidine by 2-methyl-1,4-naphthoquinone: characterization of 5-(hydroperoxymethyl)-2'-deoxycytidine and stable methyl group oxidation products. J Am Chem Soc 118:11406-11411. https://doi.org/10.1021/ja962073h

64. Lendzian F, Mobius K, Lubitz W (1982) The pheophytin a anion radical. ^{14}N and ^{1}H endor and triple resonance in liquid solution. Chem Phys Lett.90:375-381. https://doi.org/10.1016/0009-2614(82)83073-X
65. Pospíšil P, Arató A, Krieger-Liszkay A, Rutherford AW (2004) Hydroxyl radical generation by Photosystem II. Biochemistry 43:6783-6792. https://doi.org/10.1021/bi036219i
66. Krieger-Liszkay A (2005) Singlet oxygen production in photosynthesis. J Exp Bot 56:337-346. https://doi.org/10.1093/jxb/erh237
67. Pospíšil P (2009) Production of reactive oxygen species by photosystem II. Biochim Biophys Acta Bioenerg 1787:1151-1160 . https://doi.org/10.1016/j.bbabio.2009.05.005
68. Knaff DB (1975) The effect of pH on the midpoint oxidation-reduction potentials of components associated with plant photosystem II. FEBS Lett 60:331-335. https://doi.org/10.1016/0014-5793(75)80742-3
69. Klimov VV (1981) Pheophytin as the primary electron acceptor in photosystem II reaction centres. Photosynthetica 15:592-609.
70. Tanaka A, Ito H, Tanaka R, Tanaka NK, Yoshida K, Okada K (1998) Chlorophyll *a* oxygenase *(CAO)* is involved in chlorophyll *b* formation from chlorophyll *a.* Proc Natl Acad Sci U.S.A. 95:12719-12723. https://doi.org/ 10.1073/pnas.95.21.12719
71. Abe T, Tanaka S, Ogawa A, Tamura M, Sato K, Itoh S (2017) Copper-catalyzed selective oxygenation of methyl and benzyl substituents in pyridine with O_2. Adv Synth Catal 46:348-350. https://doi.org/10.1246/cl.161074
72. Ye R, Cao Y, Xi X, Liu L, Chen T (2019) Metal- and radical-free aerobic oxidation of heteroaromatic methanes: an efficient synthesis of heteroaromatic aldehydes. Org Biomol Chem 17:4220-4224. https://doi.org/10.1039/C9OB00490D
73. Chen GX, Kazimir J, Cheniae GM (1992) Photoinhibition of hydroxylamine-extracted photosystem II membranes: studies of the mechanism. Biochemistry 31:11072-11083. https://doi.org/10.1021/bi00160a017
74. Eckert HJ, Geiken B, Bernarding J, Napiwotzki A, Eichler HJ, Renger G (1991) Two sites of photoinhibition of the electron transfer in oxygen evolving and Tris-treated PS II membrane fragments from spinach. Photosyn Res 27:97-108. https://doi.org/10.1007/BF00033249
75. Blubaugh DJ, Atamian M, Babcock GT, Golbeck JH, Cheniae GM (1991) Photoinhibition of hydroxylamine-extracted photosystem II membranes: identification of the sites of photodamage. Biochemistry 30:7586-7597. https://doi.org/ 10.1021/bi00244a030
76. Tyystjärvi E (2008) Photoinhibition of Photosystem II and photodamage of the oxygen evolving manganese cluster. Coord Chem Rev 252:361-376. https://doi.org/10.1016/j.ccr.2007.08.021
77. Taguchi F, Yamamoto Y, Satoh K (1995) Recognition of the structure around the site of cleavage by the carboxyl-terminal processing protease for D1 precursor protein of the Photosystem II reaction center. J Biol Chem 270:10711-10716. https://doi.org/10.1074/jbc.270.18.10711
78. Conjeaud H, Mathis P (1980) The effect of pH on the reduction kinetics of P-680 in tris-treated chloroplasts. Biochim Biophys Acta Bioenerg 590:353-359. https://doi.org/10.1016/0005-2728(80)90206-6
79. Styring S, Sjöholm J, Mamedov F (2012) Two tyrosines that changed the world: Interfacing the oxidizing power of photochemistry to water splitting in photosystem II. Biochim Biophys Acta Bioenerg 1817:76-87. https://doi.org/10.1016/j.bbabio.2011.03.016.